

# Optical and electrical properties of high-quality $\text{Ti}_2\text{O}_3$ epitaxial film grown on sapphire substrate

Haibo Fan<sup>1,2</sup> · Mingzi Wang<sup>2</sup> · Zhou Yang<sup>1</sup> · Xianpei Ren<sup>1</sup> · Mingli Yin<sup>1,3</sup> · Shengzhong Liu<sup>1,4</sup>

Received: 4 May 2016 / Accepted: 2 September 2016 / Published online: 19 October 2016  
© Springer-Verlag Berlin Heidelberg 2016

**Abstract** Epitaxial film of  $\text{Ti}_2\text{O}_3$  with high crystalline quality was grown on  $\text{Al}_2\text{O}_3$  substrate by pulsed laser deposition process using a powder-pressed  $\text{TiO}_2$  target in active  $\text{O}_2$  flow. X-ray diffraction clearly reveals the (0006) crystalline  $\text{Ti}_2\text{O}_3$  orientation and its  $(10\bar{1}0)_{\text{Ti}_2\text{O}_3} \parallel (10\bar{1}0)_{\text{sapphire}}$  in-plane epitaxial relationship with the substrate. Scanning electron microscopy images show that the film grew uniformly on the substrate with a Volmer–Weber mode. High-resolution transmission electron microscopy and selected area electron diffraction further confirm the high crystalline quality of the film. Transmittance spectrum shows that the  $\text{Ti}_2\text{O}_3$  film is highly transparent in 400–800 nm with the optical band gap estimated to be 3.53 eV by Tauc plot. The temperature-dependent Hall effect measurement indicates that the  $\text{Ti}_2\text{O}_3$  film

appears to be *n*-type semiconductor with carrier concentration, mobility, and resistivity showing typical temperature-dependent behavior. The donor ionization energy was estimated to be 83.6 meV by linear relationship of conductivity versus temperature.

## 1 Introduction

Magneli phases [1], a series of nonstoichiometric titanium oxides with a generic formula  $\text{Ti}_n\text{O}_{2n-1}$  ( $2 \leq n \leq 10$ ), have long been in the spotlight of research for its novel electronic property [2–5] and thermoelectric characteristics [6–8]. In general, stoichiometric  $\text{TiO}_2$  is a good insulator, nonstoichiometric phases of either oxygen-rich or oxygen-deficient induce carriers, resulting in significant conductivity [9]. According to Bartholomew and Fankl who investigated systematically the electrical properties of single-crystalline magneli-phased titanium oxides, magneli oxides are metallic with electrical resistivity decreasing with the oxygen deficiency [10].

In particular,  $\text{Ti}_2\text{O}_3$  has attracted great attention over the past half century [11–14] for its semiconductor–metal transition at temperature over 200 °C, at which its resistivity dramatically decreases by several orders of magnitude [15, 16]. The generally accepted model for the  $\text{Ti}_2\text{O}_3$  semiconductor–metal transition involves a band-crossing mechanism [11]. According to the model, a small gap between filled and emptied bands in the low temperature band structure is gradually narrowed and closes as the transition takes place. Since the bands which cross are involved in metal–metal bonding, specific changes in Ti–Ti separations should accompany the electronic transition. Namely, metal–metal bonds parallel to the hexagonal *c*-axis should increase, while the metal–metal bonds in the

✉ Haibo Fan  
hbfan@snnu.edu.cn

✉ Shengzhong Liu  
liusz@snnu.edu.cn

<sup>1</sup> Key Laboratory of Applied Surface and Colloid Chemistry, National Ministry of Education, Shaanxi Engineering Lab for Advanced Energy Technology, School of Materials Science and Engineering, Shaanxi Normal University, Xi'an 710119, China

<sup>2</sup> School of Physics, Northwest University, Xi'an 710069, China

<sup>3</sup> School of Science, Xi'an Technological University, Xi'an 710062, Shaanxi, China

<sup>4</sup> Dalian Institute of Chemical Physics, Dalian National Laboratory for Clean Energy, Chinese Academy of Sciences, Dalian 116023, China

basal plane should decrease as  $\text{Ti}_2\text{O}_3$  is heated. Based on this property,  $\text{Ti}_2\text{O}_3$  is a promising candidate material for smart windows [17], thread guides [18], thermal memory [19], thermochromic materials [20], and photocatalyst [21, 22].

Although the properties of  $\text{Ti}_2\text{O}_3$  have been widely investigated, the most are based on single bulk crystal or nanopowder. There have been no reports on  $\text{Ti}_2\text{O}_3$  thin films, neither on its preparation, nor its property study. Merlin and Perry [23] firstly obtained amorphous  $\text{Ti}_2\text{O}_3$  film by cw laser irradiation of  $\text{Ti}_{50}\text{Zr}_{10}\text{Be}_{40}$  exposed to oxygen at low partial pressure. Bayati et al. [24] found that a  $\text{Ti}_2\text{O}_3$  transient layer formed during the domain epitaxy of  $\text{TiO}_2$  film on  $\text{Al}_2\text{O}_3$  substrate. In this work, thick  $\text{Ti}_2\text{O}_3$  film with high quality was epitaxially grown on sapphire substrate by a pulsed laser deposition technique with its optical and electrical properties thoroughly investigated. It is expected that these results are useful in designing  $\text{Ti}_2\text{O}_3$ -based optical and electronic devices.

## 2 Experimental

$\text{Ti}_2\text{O}_3$  film was prepared in a stainless steel vacuum chamber. A  $\text{TiO}_2$  ceramics target (99.99 % purity) was ablated by a KrF excimer laser (wavelength = 248 nm, pulse width = 20 ns) with a typical laser fluence  $5 \text{ J/cm}^2$  and a repetition of 5 Hz. The oxygen gas flow and the oxygen partial pressure were optimized to set at 30 ml/min and 0.5 Pa, respectively, during the deposition. The sapphire substrate was 4 cm away from the target, and the deposition temperature was kept at  $500 \text{ }^\circ\text{C}$ . Before deposition, the substrates were sequentially cleaned in acetone,

ethanol, and distilled water each for 30 min to remove carbon contaminants from the surfaces, before being dried by nitrogen gas. The typical deposition rate for the film was  $0.01 \text{ nm/pulse}$ .

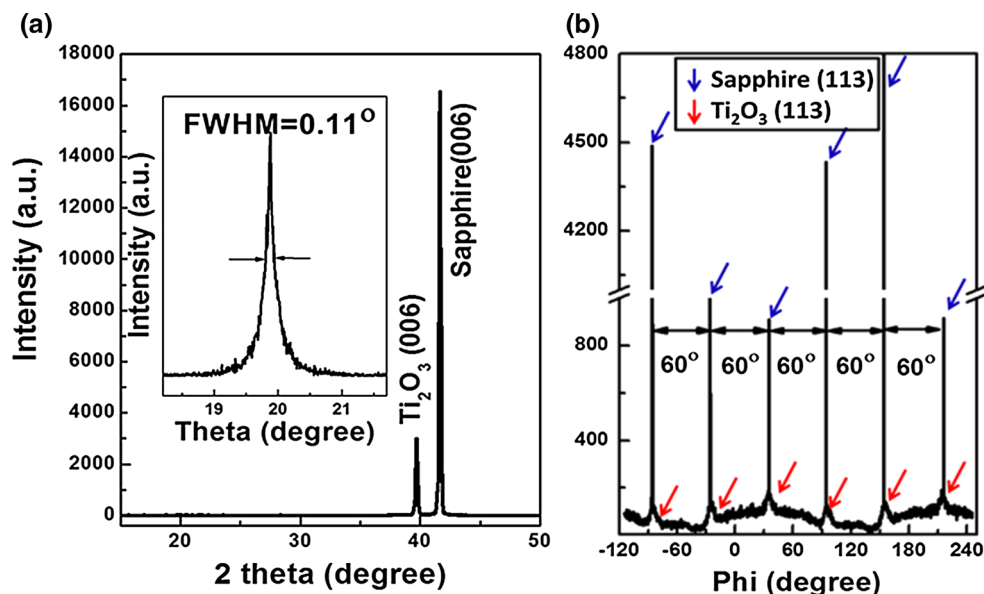
The in-plane and out-of-plane orientations of the  $\text{Ti}_2\text{O}_3$  film was characterized by  $\theta - 2\theta$  scan,  $\theta$ -rocking curve, and  $\varphi$  scan using a PANalytical X'Pert Pro X-ray diffractometer (XRD). Specimen for transmission electron microscope (TEM) observation was firstly mechanically polished and dimpled to an  $\sim 20\text{-}\mu\text{m}$ -thick disk and further thinned by neutralized ion milling. An optical study has been performed using an UV-Vis-NIR spectrophotometer at room temperature. Hall effect measurements were taken using a Lake Share 7707A equipment, and the van der Pauw method was used. The sample was cooled in a continuous He flow cryostat equipped with a magnet providing a field of 0.7 T for Hall measurements, and the measurements were taken under vacuum of about  $10^{-3}$  Torr.

## 3 Results and discussion

### 3.1 Crystal characterization

The crystalline orientation as determined by XRD  $\theta - 2\theta$  scan is shown in Fig. 1a for  $\text{Ti}_2\text{O}_3$  film deposition on sapphire substrate by PLD. This scan was performed on 200-nm-thick  $\text{Ti}_2\text{O}_3$  film. A preferential orientation of  $\text{Ti}_2\text{O}_3$  in (0006) plane is inferred based on the strong peak at  $39.699^\circ$ , which yields a  $d$  spacing of  $2.268 \text{ \AA}$ , in agreement with the lattice constant of  $\text{Ti}_2\text{O}_3$  ( $c = 6 d = 13.6 \text{ \AA}$ ). This value equals to that of bulk  $\text{Ti}_2\text{O}_3$  [24], indicating the epitaxial strain was fully relaxed. Hence, the

**Fig. 1** a  $\theta/2\theta$  XRD and b  $\varphi$  scan patterns of the  $\text{Ti}_2\text{O}_3$ /sapphire heterostructure



out-of-plane alignment of the Ti<sub>2</sub>O<sub>3</sub> film is expressed as  $(0006)_{\text{Ti}_2\text{O}_3} \parallel (0001)_{\text{sapphire}}$ . Meanwhile, XRD  $\theta$ -rocking curve measurement was also taken to investigate the degree of alignment to the normal direction of the surface. The inset of Fig. 1a shows the rocking curve data of Ti<sub>2</sub>O<sub>3</sub> (0006) plane, indicating a full width at half maximum (FWHM) value of 0.11°. Typically, heteroepitaxial semiconductor films grown on sapphire (0001) substrates show a narrow FWHM in the range of 0.1°–1°. The narrow FWHM in the XRD rocking curve implies that the *c* axis of Ti<sub>2</sub>O<sub>3</sub> film is well oriented along the normal direction of the substrate surface. Figure 1b depicts the  $\varphi$  scan pattern performed on (113) reflection of Ti<sub>2</sub>O<sub>3</sub> film (marked with red arrows) and sapphire substrate (marked with blue arrows), where six symmetrical peaks appear with azimuthal interval of 60°. Compared with the very narrow peaks of sapphire (113), the bottom broad peaks corresponding to Ti<sub>2</sub>O<sub>3</sub> (113) are ascribed to a high density of structural defects in the epitaxial Ti<sub>2</sub>O<sub>3</sub> film. From the location overlap of the two kinds of (113) peaks, we conclude that the in-plane epitaxial relationship across the Ti<sub>2</sub>O<sub>3</sub>/sapphire interface is  $(10\bar{1}0)_{\text{Ti}_2\text{O}_3} \parallel (10\bar{1}0)_{\text{sapphire}}$ , which is consistent with the TEM analysis [25], indicating that there is no rotation of the Ti<sub>2</sub>O<sub>3</sub> unit cell with respect to that of sapphire. This result is also compatible with Bayati's report, where Ti<sub>2</sub>O<sub>3</sub> only exists as a transient layer in the initial several monolayers and then acts as a template for the later growth of rutile TiO<sub>2</sub> [24]. We believe this change is heavily dependent on the different depositing conditions, such as oxygen pressure and pulse rate.

### 3.2 Film morphology

Figure 2a shows the surface morphology of the Ti<sub>2</sub>O<sub>3</sub> film, with a very flat surface with randomly distributed 40–50 nm nanoparticles. Figure 2b shows the crosssection of the Ti<sub>2</sub>O<sub>3</sub> epilayer with an abrupt interface with the sapphire substrate and a uniform thickness 200 nm. The

surface morphology may illustrate the growth mechanism by Volmer–Weber (VW) mode [26], which is usually used to interpret the semiconductor film heteroepitaxy of lattice mismatch system. Both Ti<sub>2</sub>O<sub>3</sub> and sapphire have the same corundum structure, while the lattice parameters are  $a = b = 5.15 \text{ \AA}$ ,  $c = 13.61 \text{ \AA}$  and  $a = b = 4.79 \text{ \AA}$ ,  $c = 12.99 \text{ \AA}$ , respectively. Epitaxy of Ti<sub>2</sub>O<sub>3</sub> on sapphire substrate belongs to large mismatched heteroepitaxy [27, 28]. The microstructural stages in the VW growth mode include the following steps: nucleation of discrete islands, island growth, island impingement and coalescence, percolation of the island array, and channel filling to eventually form a continuous thin film. For the case of Ti<sub>2</sub>O<sub>3</sub> grown on sapphire, the particles distributed in the film surface are the Ti<sub>2</sub>O<sub>3</sub> islands which had not yet coalesced due to the interruption of the growth process.

The crystal structure of the Ti<sub>2</sub>O<sub>3</sub> film is further examined by TEM. Figure 3a shows the low magnification superficial TEM images of the epitaxial Ti<sub>2</sub>O<sub>3</sub> film, with an apparent mosaic structure. This polycrystalline structure is consistent with the VW growth mode mentioned above. The large-scale high-resolution images are shown in Fig. 3b, from which the clear lattice fringes confirm the high crystallinity of the Ti<sub>2</sub>O<sub>3</sub> film. The lattice stripes in Fig. 3c, measured as 0.25 nm, represent the stripe image of the (110) Ti<sub>2</sub>O<sub>3</sub> plane. The selected area electron diffraction pattern is shown in Fig. 3d, in which the electron beam was parallel to the [0001] direction of the substrate. The diffraction spots are indexed as (000), (006), and (012) diffraction of the Ti<sub>2</sub>O<sub>3</sub> [24].

### 3.3 Optical properties

Figure 4a shows the UV–Vis optical transmittance spectrum of the Ti<sub>2</sub>O<sub>3</sub> film. Note that the sapphire substrate was used as the reference, and its transmittance was subtracted before testing Ti<sub>2</sub>O<sub>3</sub> film samples. The fluctuation of transmittance is believed to be related to the optical

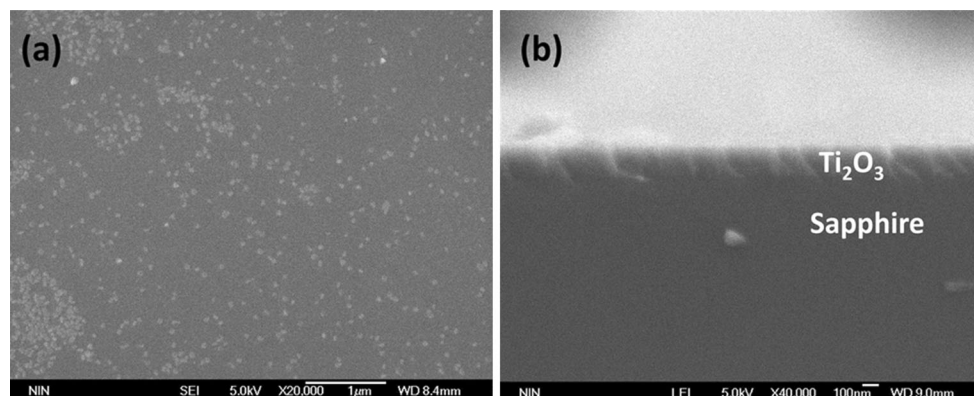


**Fig. 2** SEM images show the surface morphology (a) and crosssection (b) morphology of the Ti<sub>2</sub>O<sub>3</sub> epilayer with a thickness around 200 nm

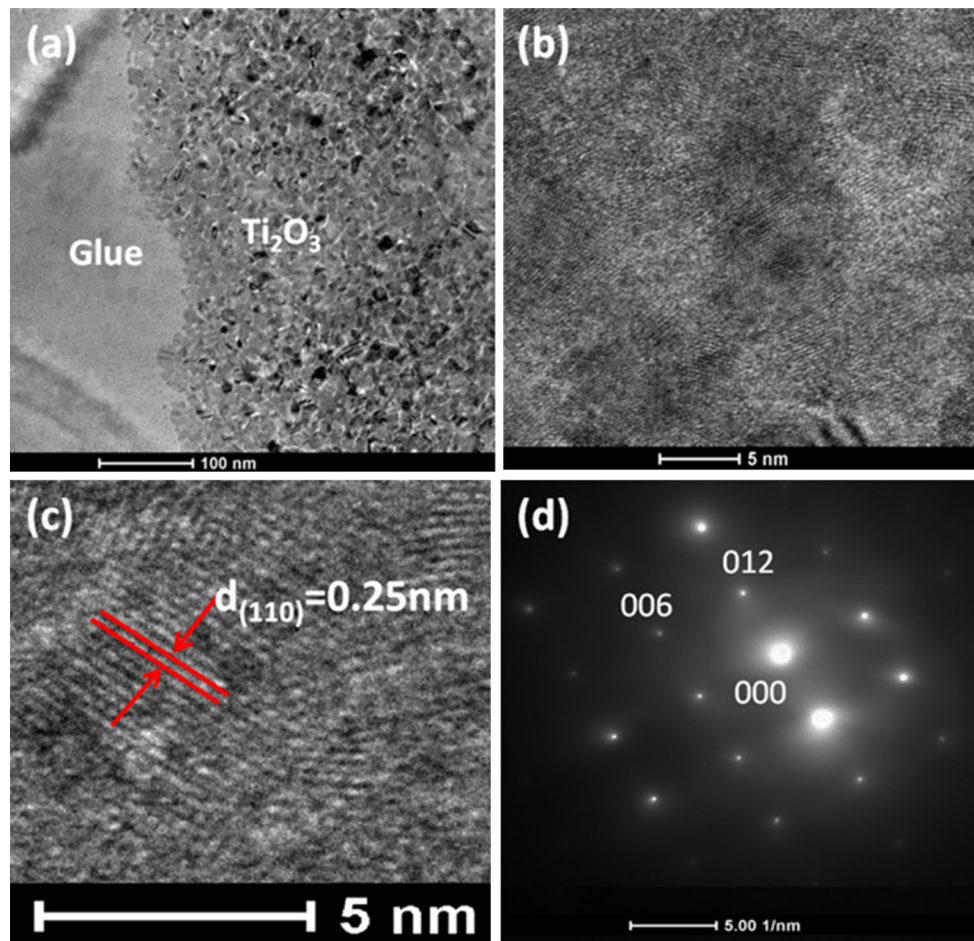


**Fig. 3** **a** TEM micrographs of bright field image for the  $\text{Ti}_2\text{O}_3$ /sapphire epitaxial film, high-resolution image in **b** low, **c** high magnification, and **d** selected area electron diffraction pattern

interference between two interfaces: air–film and film–substrate [29]. The  $\text{Ti}_2\text{O}_3$  exhibits a high optical transparency of approximate 80 % in the visible region, in good agreement with that of amorphous  $\text{Ti}_2\text{O}_3$  film prepared by electron beam evaporation [31] and comparable to that of the  $\text{TiO}_2$  film reported [31, 32]. The absorbance spectrum of the  $\text{Ti}_2\text{O}_3$  film is shown in Fig. 4b, from which an abrupt onset edge is observed. The linear function between  $(\alpha hv)^{1/2}$  versus  $hv$  indicates the existence of the allowed indirect transition. The band gap can be estimated with equation  $(\alpha hv)^{1/2} = k(hv - E_g)$  [30], in which  $\alpha$  denotes absorption coefficient,  $k$  is a constant, and  $E_g$  is the band gap energy. Plotting  $(\alpha hv)^{1/2}$  versus  $hv$  based on absorbance spectrum yields an extrapolated intercept corresponding to the value of  $E_g$  as shown in the inset of Fig. 4b. The estimated band gap of  $\text{Ti}_2\text{O}_3$  film is 3.53 eV, in good agreement with the reported value (3.58 eV) obtained from Wemple–Didomenico model while it is indeed a little larger than that (3.17 eV) calculated in terms of Tauc method [30]. It should be noted that these values are much

larger than that of bulk  $\text{Ti}_2\text{O}_3$  (0.1–0.2 eV) obtained by the activation energy from the temperature-dependent conductivity measurement [33–35].

### 3.4 Electrical properties

The temperature-dependent Hall effect was used to investigate the electrical properties. The negative Hall coefficients show that the  $\text{Ti}_2\text{O}_3$  film always exhibits *n*-type conductivity in whole temperature range. The temperature-dependent carrier concentration and mobility for  $\text{Ti}_2\text{O}_3$  film are shown in Fig. 5a, from which a strong exponential increase in carrier concentration (*n*) is seen from 50 K to 140 K. When temperature is above 140 K, the carrier concentration increases slowly until it reaches the saturation. However, the Hall mobility has been found to change in the opposite trend. When temperature is below 140 K, the mobility decreases sharply and after that it starts to oscillate with the temperature change. This phenomenon can be interpreted by the scattering mechanism of the electrons, as the mobility of electrons is limited primarily

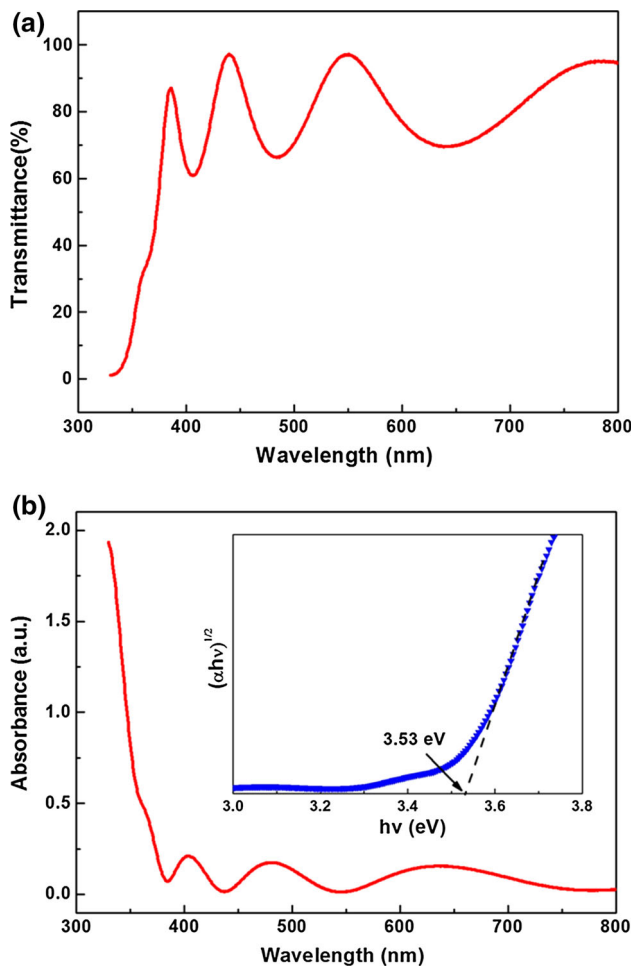


**Fig. 4** UV-Vis transmittance **a** and absorbance **b** spectra of Ti<sub>2</sub>O<sub>3</sub> film

by scattering due to ionic impurities and lattice vibrations [36]. When temperature is low (<140 K), both the donor ionization and the scattering from the lattice vibrations are low, leading to low mobility with a decreasing trend with increased temperature. When temperature is increased above 140 K, the donor ionizations are enhanced and the carrier concentration increases to a greater value. In this case, the ionized donors start to dominate the scattering mechanism, making the electron mobility decrease as the temperature increase. At the room temperature, the carrier concentration is up to  $8.62 \times 10^{19} \text{ cm}^{-3}$ , while the mobility is only  $0.15 \text{ cm}^2/\text{Vs}$ , indicating that it is related to the thin film thickness [36]. Figure 5b shows the temperature-dependent resistivity ( $\rho$ ) of the Ti<sub>2</sub>O<sub>3</sub> film. With increasing the temperature from 50 to 303 K,  $\rho$  decreases from  $15.72$  to  $5.35 \times 10^{-3} \text{ } \Omega\text{m}$ . The latter value is in good agreement with the golden Th<sub>2</sub>S<sub>3</sub>-type polymorph of the Ti<sub>2</sub>O<sub>3</sub>, a transition phase from corundum under high-pressure and high-temperature conditions [37]. It is well known that the electrical conductivity ( $\sigma$ ) is the product of

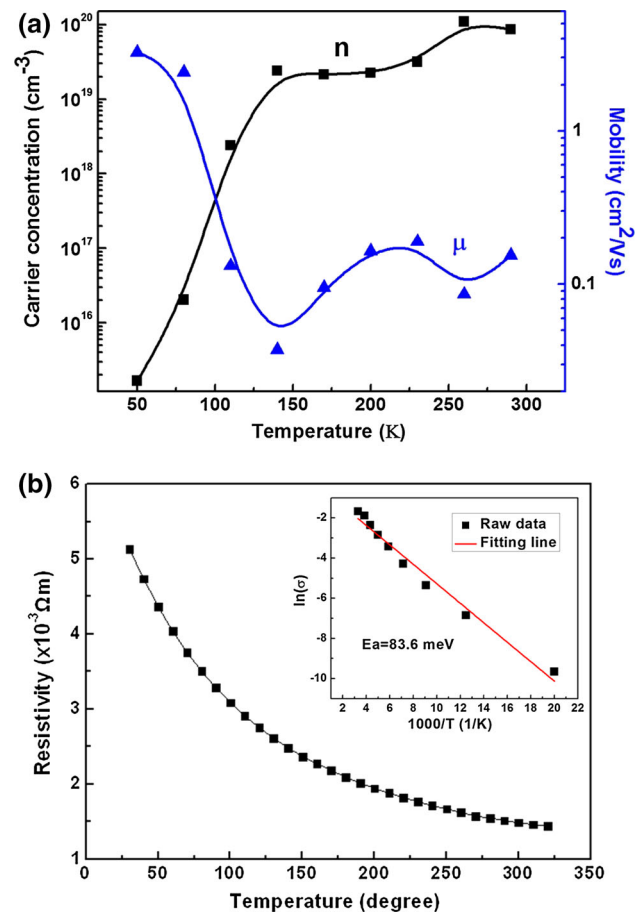


**Fig. 5** Temperature-dependent **a** carrier concentration, mobility and **b** electrical resistivity. The inset shows the plotting of  $\ln(\sigma)$  versus  $(1000/T)$ , from which the donor ionization energy ( $E_a$ ) was estimated to be 83.6 meV

the carrier concentration ( $n$ ), mobility ( $\mu$ ), and electrical charge of the carriers ( $q$ ), as defined in Eq. (1).

$$\sigma = 1/\rho = nq\mu \quad (1)$$

We find that the  $\sigma$  and  $n$  have the same variation tendency, indicating that the carrier concentration plays an important role in the resistivity variation dependent on the temperature. Electrical conductivity of the Ti<sub>2</sub>O<sub>3</sub> film at low temperatures can generally be described by a well-established theoretic relation [38]:

$$\sigma = A \exp(-B/kT), \quad (2)$$

where  $A$  is a constant,  $B$  is equal to a half of the ionization energy of a donor ( $E_d/2$ ), if we consider the single-level impurity semiconductor model as proposed by Wilson. The inset of Fig. 5b shows the plotting of  $\ln(\sigma)$  versus  $(1000/T)$ , in which a linear relationship was accepted and this is consistent with the theory prediction as shown in Eq. (2). From the slope of the fitting line, we can deduce the donor ionization energy of Ti<sub>2</sub>O<sub>3</sub> film is about 83.6 meV. Because no external dopant was deliberately introduced,

we think the underlying donor energy level may be from some native defects due to its tendency for oxygen deficiency in the film growth process, such as oxygen vacancies or metal (titanium) interstitials, which are usually responsible for the *n*-type conductivity in metal oxide wide gap semiconductors, for instance, ZnO [39] and TiO<sub>2</sub> [40]. However, the possible candidate of ubiquitous hydrogen also cannot be excluded [41]. In order to solve the problem clearly, some specific work should be carried out further.

## 4 Conclusions

In conclusion, epitaxial film of Ti<sub>2</sub>O<sub>3</sub> with high crystalline quality was grown on Al<sub>2</sub>O<sub>3</sub> substrate using a PLD process with a powder-pressed TiO<sub>2</sub> target in an optimized condition. XRD patterns reveal that the high crystalline quality of the Ti<sub>2</sub>O<sub>3</sub> film. The out-of-plane alignment of the Ti<sub>2</sub>O<sub>3</sub>/sapphire was expressed as (0006)<sub>Ti<sub>2</sub>O<sub>3</sub></sub> || (0001)<sub>sapphire</sub>, and the in-plane epitaxial relationship across the interface is (10 $\bar{1}$ 0)<sub>Ti<sub>2</sub>O<sub>3</sub></sub> || (10 $\bar{1}$ 0)<sub>sapphire</sub>. Scanning electron microscopy (SEM) images reveal that the film grew smoothly on the substrate with a VW mode. High-resolution TEM and SAED were used to verify the high crystalline quality of the film. Transmittance spectrum shows that the Ti<sub>2</sub>O<sub>3</sub> film has good optical transmittance and the band gap was estimated to be 3.53 eV by the absorbance spectrum. Temperature-dependent Hall effect measurement indicates that Ti<sub>2</sub>O<sub>3</sub> appears to be *n*-type semiconductor through the entire temperature range. At room temperature, the carrier concentration is up to  $8.62 \times 10^{19} \text{ cm}^{-3}$ , while the mobility was 0.15 cm<sup>2</sup>/Vs. Fitting the linear relationship of conductivity and temperature, the donor ionization energy of Ti<sub>2</sub>O<sub>3</sub> film was estimated to be about 83.6 meV. It is expected that these results are useful for future designing and preparing of Ti<sub>2</sub>O<sub>3</sub>-based optical and electronic devices.

**Acknowledgments** The authors acknowledge the support from Shaanxi postdoctoral scientific research projects, the National Natural Science Foundation (11204238), National University Research Fund (GK261001009), the Changjiang Scholar and Innovative Research Team (IRT\_14R33), the Overseas Talent Recruitment Project (B14041) and the Chinese National 1000-talent-plan program. Haibo Fan wishes to thank Prof. Jingwen Zhang for the help of Hall effect measurements.

## References

1. S. Andersson, B. Collén, U. Kuylenstierna, A. Magnéli, *Acta Chem. Scand.* **11**, 1641 (1957)
2. J.P. Strachan, M.D. Pickett, J.J. Yang, S. Aloni, A.L. David Kilcoyne, G. Medeiros-Ribeiro, R. Stanley Williams, *Adv. Mater.* **22**, 3573 (2010)
3. D.H. Kwon, K.M. Kim, J.H. Jang, J.M. Jeon, M.H. Lee, G.H. Kim, C.S. Hwang, *Nat. Nanotechnol.* **5**, 148 (2010)
4. M. Canillas, E. Chinarro, M. Carballo-Vila, J.R. Jurado, B. Moreno, *J. Mater. Chem. B* **1**, 6459 (2013)
5. V. Adamaki, F. Clemens, P. Ragulis, S.R. Pennock, J. Taylor, C.R. Bowen, *J. Mater. Chem. A* **2**, 8328 (2014)
6. N. Okinaka, T. Akiyama, *Jpn. J. Appl. Phys.* **45**, 7009 (2006)
7. Q. He, Q. Hao, G. Chen, B. Poudel, X. Wang, D. Wang, Z. Ren, *Appl. Phys. Lett.* **91**, 52505 (2007)
8. N.V. Morozova, I.A. Khmeleva, S.V. Ovsyannikov, A.E. Karkin, V.V. Shchennikov, *Phys. Stat. Sol. (b)* **250**, 741 (2013)
9. U. Diebold, *Surf. Sci. Rep.* **48**, 53 (2003)
10. R.F. Bartholomew, D.R. Fankl, *Phys. Rev.* **187**, 828 (1969)
11. C.E. Rice, W.R. Robinson, *Acta Crystallogr. Sect. B* **33**, 1342 (1977)
12. J.B. Goodenough, *Phys. Rev.* **117**, 1442 (1960)
13. A.I. Poteryaev, A.I. Lichtenstein, G. Kotliar, *Phys. Rev. Lett.* **93**, 086401 (2004)
14. M. Taguchi, A. Chainani, M. Matsunami, R. Eguchi, Y. Takata, M. Yabashi, S. Shin, *Phys. Rev. Lett.* **104**, 106401 (2010)
15. F.J. Morin, *Phys. Rev. Lett.* **3**, 34 (1959)
16. W. Yan, M. Fang, M. Liu, S. Kang, R. Wang, L. Zhang, L. Liu, J. Appl. Phys. **111**, 123509 (2012)
17. R. Lopez, L.C. Feldman, R.F. Haglund Jr., *Phys. Rev. Lett.* **93**, 177403 (2004)
18. See <http://www.designinsite.dk/htmsider/inspmat.htm> for the application of Ti<sub>2</sub>O<sub>3</sub> in thread guides
19. See <http://priorartdatabase.com/IPCOM/000063571> for the application of Ti<sub>2</sub>O<sub>3</sub> in thermal memory
20. P. Kiri, G. Hyett, R. Binions, *Adv. Mater. Lett.* **1**, 86 (2010)
21. M. Uno, S. Nishimoto, Y. Kameshima, M. Miyake, *Int. J. Hydrog. Energy* **38**, 15049 (2013)
22. J. Wang, P. Yang, B. Huang, *Appl. Surf. Sci.* **356**, 391 (2015)
23. R. Merlin, T.A. Perry, *Appl. Phys. Lett.* **45**, 852 (1984)
24. M.R. Bayati, R. Molaei, R.J. Narayan, *Appl. Phys. Lett.* **100**, 251606 (2012)
25. T. Fujii, N. Sakata, J. Takada, Y. Miura, Y. Daitoh, M. Takano, *J. Mater. Res.* **9**, 1468 (1994)
26. J.A. Floro, S.J. Hearne, J.A. Hunter, P. Kotula, E. Chason, S.C. Seel, C.V. Thompson, *J. Appl. Phys.* **89**, 4886 (2001)
27. J.H. Van der Merwe, *J. Appl. Phys.* **34**, 123 (1962)
28. J.W. Matthews, S. Mader, T.B. Light, *J. Appl. Phys.* **41**, 3800 (1970)
29. G. Papadimitropoulos, N. Vourdas, K. Giannakopoulos, M. Vasilopoulou, D. Davazoglou, *J. Appl. Phys.* **109**, 103527 (2011)
30. M.M. Abdel-Aziz, I.S. Yahia, L.A. Wahab, M. Fadel, M.A. Affif, *Appl. Surf. Sci.* **252**, 8163 (2006)
31. D.J. Won, C.H. Wang, H.K. Jang, D.J. Choi, *Appl. Phys. A* **73**, 595 (2001)
32. T. Watanabe, S. Fukayama, M. Miyauchi, A. Fujishima, K. Hashimoto, *J. Sol gel Sci. Technol.* **19**, 71 (2000)
33. S.V. Ovsyannikov, X. Wu, A.E. Karkin, V.V. Shchennikov, G.M. Manthilake, *Phys. Rev. B* **86**, 024106 (2012)
34. S.H. Shin, G.V. Chandrashekar, R.E. Loehman, J.M. Honig, *Phys. Rev. B* **8**, 1364 (1973)
35. T.C. Chi, R.J. Sladek, *Phys. Rev. B* **7**, 5080 (1973)
36. K.T. Roro, G.H. Kassier, J.K. Dangbegnon, S. Sivaraya, J.E. Westraadt, J.H. Neethling, J.R. Botha, *Semicond. Sci. Technol.* **23**, 055021 (2008)
37. S.V. Ovsyannikov, X. Wu, G. Garbarino, M. Nunez-Regueiro, V.V. Shchennikov, J.A. Khmeleva, L. Dubrovinsky, *Phys. Rev. B* **88**, 184106 (2013)
38. S.E. Harrison, *Phys. Rev.* **93**, 52 (1954)
39. L. Schmidt-Mende, J.L. MacManus-Driscoll, *Mater. Today* **10**, 40 (2007)
40. B.J. Morgan, G.W. Watson, *J. Phys. Chem. C* **114**, 2321 (2010)
41. C.G. Van de Walle, *Phys. Rev. Lett.* **85**, 1012 (2000)